Received: 5 December 2022 | Revised: 27 February 2023 | Accepted: 22 March 2023

DOI: 10.1002/pol.20220719

RESEARCH ARTICLE

JOURNAL OF POLYMER SCIENCE WILEY

Effect of isopropanol cosolvent on the rheology and spinnability of aqueous polyacrylic acid solutions

Sunilkumar Khandavalli[1] | **Yingying Chen**[1] | **Nisha Sharma-Nene**[1] | **Kashyap Sundara Rajan**[2] | **Samrat Sur**[2] | **Jonathan P. Rothstein**[2] | **Kimberley S. Reeves**[3] | **David A. Cullen**[3] | **K. C. Neyerlin**[1] | **Scott A. Mauger**[1] | **Michael Ulsh**[1]

[1]Chemistry and Nanoscience Center, National Renewable Energy Laboratory, Golden, Colorado, USA

[2]Mechanical and Industrial Engineering, University of Massachusetts, Amherst, Massachusetts, USA

[3]Center for Nanophase Materials Sciences, Oak Ridge National Laboratory, Oak Ridge, Tennessee, USA

Correspondence
Sunilkumar Khandavalli, Chemistry and Nanoscience Center, National Renewable Energy Laboratory, Golden, CO 80401, USA.
Email: sunilkumar.khandavalli@nrel.gov

Funding information
U.S. DOE, Office of Energy Efficiency and Renewable Energy, Advanced Manufacturing Office

Abstract

We investigate the effect of alcohol fraction (isopropanol, IPA) in a binary water-alcohol solvent mixture on the shear and extensional rheological properties, as well as the role of viscoelasticity on fiber formation of poly(acrylic acid) (PAA) in electrospinning. Comparison of the scaling of both specific viscosities η_{sp} and extensional relaxation times λ_E of PAA in water–IPA mixtures, showed stronger scaling compared to salt-free aqueous polyelectrolyte solutions, except for the η_{sp} in the unentangled regime displaying a polyelectrolyte-like scaling $\eta_{sp} \sim c^{0.5}$ for all IPA%. Such deviation suggested IPA induces association/aggregation of PAA. However, the trends between η_{sp} and λ_E magnitudes as a function of IPA% differ for concentrations compared in the entangled regime. The η_{sp} as well as their elastic moduli exhibit a maximum, whereas λ_E increases monotonically with IPA%, suggesting a complex interplay of various interactions are dictating their structure in water-IPA mixtures, affecting their shear and extensional response differently. Electrospinning experiments showed increasing IPA% reduces the onset of both beaded and uniform fibers. Analysis using dimensionless numbers indicated the enhancement of their elasticity by IPA, and the consequent stabilizing effect on their jets/filaments against break-up during electrospinning, plays a role in the improvement of their fiber formation.

KEYWORDS

electrospinning, extensional rheology, nanofibers, polyacrylic acid, polyelectrolytes, shear rheology

1 | INTRODUCTION

Polyelectrolytes are attractive for many applications (e.g., biomedicine,[1,2] sensors,[3] air filtration,[4] and batteries).[5] Nanofibers of polyelectrolytes, or their blends with other polymers, have gained significant interest in the recent years for many of these applications due to the large surface-area-to-volume ratio of the nanofibers and high porosity of the nanofiber mat/matrix, which have been found to enhance their functionality.[4,6,7]

This is an open access article under the terms of the Creative Commons Attribution License, which permits use, distribution and reproduction in any medium, provided the original work is properly cited.
© 2023 Alliance for Sustainable Energy, LLC and Oak Ridge National Laboratory and The Authors. *Journal of Polymer Science* published by Wiley Periodicals LLC.

Electrospinning is one of the common techniques to fabricate nanofibers because of its simplicity and the ability to fabricate nanofibers of diverse materials, and allows fabrication of ultra-thin fibers, upto 100 nm, compared to other techniques. In this technique, the polymer-containing liquid is pumped through a nozzle and elongated by applying a high voltage potential between the nozzle tip and a grounded collector. The fiber is formed by a liquid jet that emanates from the tip of a cone-shaped reservoir formed at the nozzle tip (called a Taylor cone) due to electrostatic repulsion forces of the charged ions in the fluid. The jet is significantly deformed by the electrostatic forces and, in some cases, the onset of a bending instability along the length of the jet resulting in further elongation. As the jet reaches the grounded collector, it solidifies due to solvent evaporation, resulting in the formation of thin fibers.[8–10]

The uniformity of fibers is strongly influenced by the dynamics (stability and break-up) of the jet. The jet dynamics are governed by the balance between several forces (e.g., viscous, elastic, capillary, electrostatic, and inertial). Viscoelastic forces tend to stabilize the jet against capillary break-up, promoting the evolution of uniform fibers, whereas inertia exacerbates the capillary break-up process causing the formation of beads.[11,12] Several factors such as the fluid properties, process parameters, and ambient conditions influence the magnitude of these forces, thus the jet dynamics, and in turn the fiber formation.[13]

Many studies have focused on predicting the minimum polymer concentration required to create beaded (C_{fb}) and uniform nanofibers (C_f) for both neutral[12,14–16] and charged polymers.[17–21] For neutral polymers in good solvents and with no specific interactions, at moderate to low-molecular weights where the solutions are predominantly viscous, the critical concentration for the onset of fiber formation is found to correspond to entanglement concentration C_e—the critical concentration above which the polymer begins to form chain entanglements, $C_{fb} \sim C_e$.[12,15,16] Above C_e, the buildup of solution viscosities due to chain entanglements stabilizes the jet. And the formation of uniform fibers was found to occur at concentrations beyond the entanglement concentration, $C_f \sim 2\text{–}2.3 \times C_e$.[15] However, for solutions of high-molecular weight polymers, which are highly elastic, the onset of fiber formation was found to be much lower than C_e.[14,16,22] This is because of the enhancement of their extensional viscosities by the elastic effects, which play a predominant role in the electrospinning process due to extensionally dominant nature of the process/flow. Such elastic effects in polymer solutions originate from the unraveling of the polymer coils in extensional flows above a critical stretch rate, leading to strain hardening of the extensional viscosity—where extensional viscosity increases with increasing Hencky strain. The magnitude of strain hardening increases with increasing polymer molecular weight due to an increase in the finite extensibility limit of the polymer.[23] Therefore, at high-molecular weights, a significant enhancement of the extensional viscosities relative to shear leads to the formation of fibers at concentrations below C_e without requiring chain entanglements. In contrast to polymers in good solvents and with no polymer–polymer interactions, polymers exhibiting strong specific interactions such as H-bonding/ionic interactions, or polymers in moderately poor solvent undergoing aggregation, a combination of both physical associations (reversible crosslinking/junctions) between polymer chains and chain entanglements are known to play a role in fiber formation.[24,25]

Owing to the presence of ionic groups, the properties of polyelectrolyte solutions are well-known to differ from neutral polymers. And therefore, the minimum criteria for the spinnability or fiber formation (beaded and uniform fibers) of polyelectrolyte solutions has been found to vary from that of neutral polymers.[18] Because of the dissociation of the polyelectrolytes in polar media where the counter-ions are released into the media, they are found to exhibit high electrical conductivities compared to neutral polymers.[18,26] Increasing the solution conductivity increases the magnitude of electrostatic repulsions that increase the deformation rates of the jet. The viscoelastic stresses, which build with deformation rates, resist jet deformation rates induced by the electrostatic forces. The balance between the two dictates the overall deformation rates of the jet, and thus its thinning profile. Therefore, due to the very high conductivities of polyelectrolyte solutions, strong electrostatic repulsions are found to lead to thinner fibers compared to neutral polymers, or even accelerate the break-up of the jet, when not sufficiently overcome by the viscoelastic stresses in the jet.[18]

In addition to their conductivity, the electrostatic interactions between their charged groups alter the structure of polyelectrolytes, modifying their rheological properties. The intra-chain electrostatic repulsions between the charged groups result in an extended, rod-like, structure of polyelectrolytes at dilute concentrations, referred to as polyelectrolyte-effect. Because of this effect, salt-free polyelectrolytes show a weaker zero-shear viscosity scaling with concentration, $\eta_0 \sim c^{0.5}$, compared to neutral polymers, $\eta_0 \sim c^{1.3}$, in the semi-dilute unentangled regime.[27,28] While such extended structure reduces their entanglement concentration, studies have proposed that it decreases the degree of chain entanglements compared to neutral polymers, which is shown to be one of the important criteria for the spinnability of polymer solutions.[29]

Because of these differences, studies on polyelectrolyte solutions examining the correlation between the

26424169, 2023, 14, Downloaded from https://onlinelibrary.wiley.com/doi/10.1002/pol.20220719 by National Renewable Energy Lab, Wiley Online Library on [27/07/2023]. See the Terms and Conditions (https://onlinelibrary.wiley.com/terms-and-conditions) on Wiley Online Library for rules of use; OA articles are governed by the applicable Creative Commons License

onset of fiber formation (beaded and bead-free fibers) and C_e found the onset of the fiber formation relative to the C_e to be higher compared to neutral polymers. McKee et al.[18] who have studied the spinnability of polyelectrolyte solutions (cationic poly(2-(dimethyl amino)ethyl methacrylate hydrochloride) solutions in water–methanol solvent mixtures) have observed the onset of fibers and uniform fibers to be $8 \times C_e$ and $9 \times C_e$, respectively. The larger concentrations relative to the neutral polymers have been attributed to the very high conductivities of the polyelectrolyte solutions. Subramaniam et al.,[21] who investigated spinnability of sulfonated polystyrene solutions in N,N-dimethylformamide (DMF), reported the onset of beaded-fibers and uniform fibers to be $2 \times C_e$ and $3.5 \times C_e$, respectively. Tsou et al.,[19,20] who studied spinnability of polyamide-6 solutions in a formic acid (FA)/H_2O (99/1 wt/wt) solvent mixture, did not observe uniform fibers until $7.5–8 \times C_e$. They have attributed this to insufficient entanglement density of the polyelectrolytes due to the extended-chain conformation of the polyelectrolyte solutions. Saquing et al.[17] found it was not possible to spin fibers (beaded or bead-free) from aqueous sodium alginate solutions, even at $13 \times C_e$. This has been attributed to a combination of both high conductivities and high surface tension of the solutions, and the addition of a high-molecular weight PEO carrier polymer was needed to spin fibers.

Poly(acrylic acid) (PAA), a weak anionic polyelectrolyte consisting of carboxylic acid side-chain groups, is an attractive polyelectrolyte used in many applications, such as tissue engineering,[1,2] drug delivery,[30] enzyme immobilization,[6] sensors,[3] air filtration,[4] and batteries.[5] Owing to their significance in many of these applications, several reports exist on the fabrication of electrospun PAA nanofibers[3,6,7,13,31–35] or their blends with other materials.[4,26,31,36,37] These previous studies investigated the impact of several solutions parameters—such as polymer concentration,[32,34] ionic strength,[33] solvent type,[38] cosolvent[3,34]—as well as process parameters[13,35] on their fiber morphology.

Alcohols are commonly used as a cosolvent for aqueous electrospinning formulations, both for polyelectrolyte solutions[17,26] as well as mixtures of polyelectrolytes and particles/polymers.[36,39] The addition of alcohol can alter various solution properties (volatility, interfacial tension, conductivity), including their rheological properties, which can have dramatic effect on their fiber formation. Many studies have examined the spinnability of PAA solutions in binary water-alcohol mixtures or in pure alcohols.[2,3,13,34,35] Although the focus of most these studies is at a fixed solvent composition, studies do exist examining the effect of alcohol fraction on the morphology of PAA nanofibers.[3,34] Ding et al.[3] have reported an improvement in fiber morphology (or formation of the bead-free fibers) from solutions in both ethanol/water mixtures (50/50 wt/wt) and pure ethanol compared to in water for the same PAA concentration, which is qualitatively similar to findings on neutral polymers.[40–43] They attributed the improvement to a combination of both an enhancement of shear viscosities in both ethanol and water–ethanol mixtures compared to water, and an increase in the volatility of the solvent, which leads to faster solidification of jet, and thus increases its stability. Vats et al.,[34] who examine both shear rheology and spinnability of the same system as Ding et al,[3] suggest uniform fibers can be obtained if their viscosity matched to the same shear viscosity value by adjusting the PAA concentrations, regardless of water–alcohol composition.

While the above studies show that fiber morphology can be improved with the addition of alcohol, how the alcohol composition affects the onset of fiber formation—both beaded and uniform fibers—and the role of viscoelasticity, to our knowledge, has not been studied, understanding of which is important for predicting the fiber morphologies for the solutions in water–alcohol mixtures. In the previous studies, the comparisons between different water–alcohol composition, both their solution properties and fiber morphology, are limited to very few solution conditions. Ding et al.[3] compare fiber morphologies and viscosities at only one PAA concentration. Vats et el.[34] evaluate fiber morphologies for a series of PAA concentrations to identify viscosity corresponding to uniform fibers, but only for one solvent composition (50/50 ethanol/water). For other solvent compositions compared in the study, the fiber morphologies were determined only at one solution condition (same viscosity as 50/50 ethanol/water case), assuming the minimum viscosity required for uniform fiber formation to be the same.

Furthermore, as discussed before, extensional rheological properties play an important role in the electrospinning process. Previous studies on the extensional rheology of polyelectrolyte solutions in water–alcohol mixtures, though fewer compared to in aqueous media, reported the effect of alcohol on the extensional flow properties to be distinct from shear.[44–47] Despite their importance, previous studies examining the effect of water–alcohol composition on fiber morphology of PAA solutions have only considered shear rheology in correlating to the fiber morphology, and are rarely reported even in studies on using aqueous or other media. Studies focused on extensional rheology are also fewer on polyelectrolyte solutions in water–alcohol mixtures[44–47] compared to in water/polar media.[48–51]

In this study, we examine the influence of alcohol cosolvent on the shear and extensional rheological properties, and the onset of fibers—both beaded and

26424169, 2023, 14, Downloaded from https://onlinelibrary.wiley.com/doi/10.1002/pol.20220719 by National Renewable Energy Lab, Wiley Online Library on [27/07/2023]. See the Terms and Conditions (https://onlinelibrary.wiley.com/terms-and-conditions) on Wiley Online Library for rules of use; OA articles are governed by the applicable Creative Commons License

uniform—of PAA solutions. And we analyze the relationship between the onset of fiber formation and rheological properties to understand the role of viscoelasticity on fiber formation. We use isopropanol (IPA) as an alcohol cosolvent, which is one of the common solvents in industrial formulations, and has also been used in electrospinning polymer and particle formulations for fabrication of membranes[37] and electrodes for fuel cell applications.[52,53] Previous rheological studies examining the effect alcohol cosolvent on both shear and extensional rheology of various aqueous polyelectrolyte solutions, including PAA,[44–47] used a relatively more polar alcohols (propylene glycol and glycerol, $\varepsilon_r > 36$) compared to IPA ($\varepsilon_r \sim 20$). Such studies on PAA solutions using IPA[36] or similar solvents (e.g., ethanol)[3,34] while exist, but less detailed. Here we compare the rheological properties and the fiber morphologies of the PAA solutions between three different IPA wt% in the solvent for a series of PAA concentrations. The relationship between the rheological properties and the fiber formation, and the role of viscoelasticity was analyzed using dimensionless numbers.

2 | EXPERIMENTAL

2.1 | Materials and sample preparation

Polyacrylic acid (PAA) powder was purchased from Sigma Aldrich (Mw ≈ 450,000 g/mol) and was used as-received. The charge fraction of PAA solutions in water, determined from titration of PAA solutions in D.I. water with NaOH using an auto titrator (Mettler Toledo), was nearly $f \sim 1$. Solutions were prepared by adding desired amounts of PAA to glass jars containing a solvent mixture of IPA (Sigma Aldrich) and deionized (DI) water (Milli Q- 18.2 MΩ/cm) at desired solvent compositions. The samples were allowed to mix by placing the jars on rollers for at least 3 days. Solution conductivities were measured using a conductivity meter (ThermoFisher Scientific, Orion 4-Star) at ~23 °C.

2.2 | Shear rheology

Rheological measurements were performed using a stress-controlled rheometer (Thermo-Scientific HAAKE Mars 60 Rheometer) with a stainless-steel cone-plate geometry (35 mm diameter, 2° cone angle) at a gap of 0.1 μm at 25 °C. To minimize solvent evaporation during measurements, a solvent-saturation trap was used. The samples were preconditioned to erase any sample loading history on the microstructure by conducting a pre-shear at 500 s^{-1} for 60 s, followed by a resting step for 60 s. The steady shear rheology measurements were performed by imposing an increasing rate sweep with logarithmic spacing ranging from 0.01 to 1000 s^{-1}. Frequency sweep measurements have been performed varying frequency from 5 to 0.01 Hz at a fixed strain amplitude chosen within the linear viscoelastic regime, with pre-shear protocol similar to that used for steady shear.

2.3 | Experimental, Extensional rheology

To characterize the extensional rheology of the fluids we used both Capillary Breakup Extensional Rheometry (CaBER)[54] and Dripping onto Substrate Capillary Breakup Extensional Rheometry (DoS) technique[55] (similar to our previous works). In CaBER a nearly cylindrical liquid bridge is placed between two cylindrical plates with radii of $R_i = 1.5$ mm and stretched with a constant velocity of $U = 200$ mm/s from an initial length $L_i = R_i$ to final length of L_f, where $L_f = 3\ L_i$. And the diameter decay was monitored using a laser micrometer (Omron Z4LA) with a resolution of 5 μm to obtain final Hencky strains of up to $\varepsilon_f = 12.7$, given as,

$$\epsilon = 2 \ln\left(\frac{R_i}{R_{mid}(t)}\right) \quad (1)$$

Whereas in DoS rheometry, the liquid is dispensed by a syringe pump (KD Scientific) and a liquid bridge is formed between a needle and a glass substrate by allowing a drop of liquid to drip from the needle. The diameter of the needle (D_0) was 800 μm and the volumetric flow rate (Q_0) was 0.02 mL/min. An aspect ratio of $H_0/D_0 = 3$, where H_0 is the height of the needle from the substrate, was selected to create an unstable liquid bridge as soon as the drip makes contact and spreads on the substrate. A high speed camera (Phantom-Vision optics, V-4.2) with a frame rate of 25,000 fps and resolution of 192 × 64 pixels (for most of the experiments) and a long range microscope lens (Edmund optics, ×4.5 zoom) were used to record the capillary break-up process.[23] Filament diameter was measured from the diameter decay images using an edge detection algorithm (Edgehog, KU Leuven). Diameter values below 20 μm were not reported to minimize the resolution error (±5 μm).

The diameter decay data of the test fluid obtained from both the CaBER and DoS rheometry techniques is used to calculate the extensional flow properties. The diameter decay data was fit using a spline function and differentiated to calculate the extension rates ($\dot{\epsilon}$) as,

26424169, 2023, 14, Downloaded from https://onlinelibrary.wiley.com/doi/10.1002/pol.20220719 by National Renewable Energy Lab, Wiley Online Library on [27/07/2023]. See the Terms and Conditions (https://onlinelibrary.wiley.com/terms-and-conditions) on Wiley Online Library for rules of use; OA articles are governed by the applicable Creative Commons License

$$\dot{\epsilon} = -\frac{2}{R_{mid}(t)}\frac{dR_{mid}(t)}{dt} \quad (2)$$

where R_{mid} is radius at the mid-filament. The apparent extensional viscosity was then calculated as,

$$\eta_E = \frac{2\sigma}{\frac{dR_{mid}}{dt}} \quad (3)$$

where σ is liquid surface tension, which varied between 28.9 and 22.5 mN/m with varying IPA% in the solvent mixture between 25% and 75%.[56] For a Newtonian fluid, the radius of the fluid filament will decay linearly with time, $R_{mid(t)} \sim (t_b - t)$, to the final breakup at time t_b.[56,57] And for a viscoelastic fluid, characterized by an Oldroyd-B model with a relaxation time of λ_E, the radius will decay exponentially with time, $R_{mid(t)} \sim \exp(-t/3\lambda_E)$ resulting in a constant extension rate of $\dot{\epsilon} = 2/3\lambda_E$.[58] The diameter decay data was fitted to an exponential function to extract the extensional relaxation times. The extensional viscosity was then examined as a function of Hencky strain. In DoS rheometry, the radius of the syringe tip was used as R_i for the evaluation of ϵ.

2.4 | Electrospinning technique

To fabricate nanofibers, a custom designed electrospinner was used. [ref. 36 Khandavalli et al. 2021] The fluid was pumped using a syringe pump (KDS100 Infusion Syringe Pump) into a stainless-steel needle (22-gauge, inner radius $R_0 = 0.21$ mm) at a fixed flow rate of $Q_o = 0.2$ mL/h. A high-voltage potential of 7.5 kV relative to the collector was applied at the needle tip. The collector was a stainless-steel rotating drum (100 rpm) covered with aluminum foil. The distance between the needle-tip and the collector was 10 cm. Experiments were conducted at room temperature (23 ± 2 °C) and at relatively humidity between 35% and 40% RH, controlled within the environmental chamber of the electrospinning system.

2.5 | Scanning electron microscope

Fiber morphologies were characterized using a Hitachi S-4800 scanning electron microscope (SEM). Gold was sputtered onto each sample prior to SEM characterization to reduce charging. Secondary electron images were recorded using a 5 kV accelerating voltage. The fiber diameters were determined by processing SEM images through ImageJ software.

3 | RESULTS AND DISCUSSION

3.1 | Rheology

3.1.1 | Shear rheology

Prior to analyzing the spinnability of the PAA solutions, the shear and extensional rheological properties are discussed. The specific viscosity $\eta_{sp} = (\eta_0 - \eta_s)/\eta_s$ where η_s is the solvent viscosity, of PAA solutions for a series of concentrations with different IPA wt% in the solvent, 25%, 50%, and 75%, is shown in Figure 1A–C, respectively. The η_{sp} scaling increases with increasing PAA concentration c for all IPA%, as expected. The power scaling exponents n, where $\eta_{0,r} \sim c^n$, in different concentration regimes were determined from power-law fits. At low concentrations, the scaling exponents of all three IPA% cases are between $n \sim 0.44$ and 0.48. The values are close to that of salt-free polyelectrolyte solutions $n \sim 0.5$ in the semi-dilute unentangled regime, following Fuoss' law.[27,28] Such scaling suggests an extended rod-like structure at dilute concentrations, as a result of strong intra-chain electrostatic repulsions arising from the dissociated carboxylic acid groups.[27]

With increasing IPA%, the dielectric constant (ε_r) of the solvent mixture decreases, where $\varepsilon_r \sim 60$, 44, and 31, for 25%, 50%, and 75% IPA, respectively.[59] The decrease is nearly a 2x factor between 25% and 75% IPA, and even greater, 2.5x, compared to water ($\varepsilon_r \sim 72$). One may expect such variation to affect the electrostatic interactions, given that decreasing ε_r would increase the degree of condensation of the counter-ions. Such increase would in turn reduce the magnitude of intra-chain electrostatic interactions, decreasing their chain extension, and consequently affecting their scaling behavior. The comparison of total solution conductivities Λ_t between different IPA% (Figure S1A) also confirms such a reduction in their dissociation. The Λ_t includes contribution from the dissociated counter-ions/protons, in addition to the polyions and the medium. For any given PAA concentration, the Λ_t decreased with increasing IPA%, indicating an increase in the condensation of PAA, which in turn might be expected to reduce the electrostatic repulsions.

In a previous study by Jimenez et al.,[45,46] the addition of glycerol, a less polar solvent than water, was found to indeed result in a deviation of the scaling of aqueous PAA solutions from a salt-free polyelectrolyte solutions. A similar variation was also observed for NaCMC solutions on the addition of glycerol.[45,46] Our observations here on IPA deviates from these previous reports. Similar deviations have also been reported. For strong polyelectrolyte solutions, for example, poly(sodium 4-styrenesulfonate) NaPSS

26424169, 2023, 14, Downloaded from https://onlinelibrary.wiley.com/doi/10.1002/pol.20220719 by National Renewable Energy Lab, Wiley Online Library on [27/07/2023]. See the Terms and Conditions (https://onlinelibrary.wiley.com/terms-and-conditions) on Wiley Online Library for rules of use; OA articles are governed by the applicable Creative Commons License

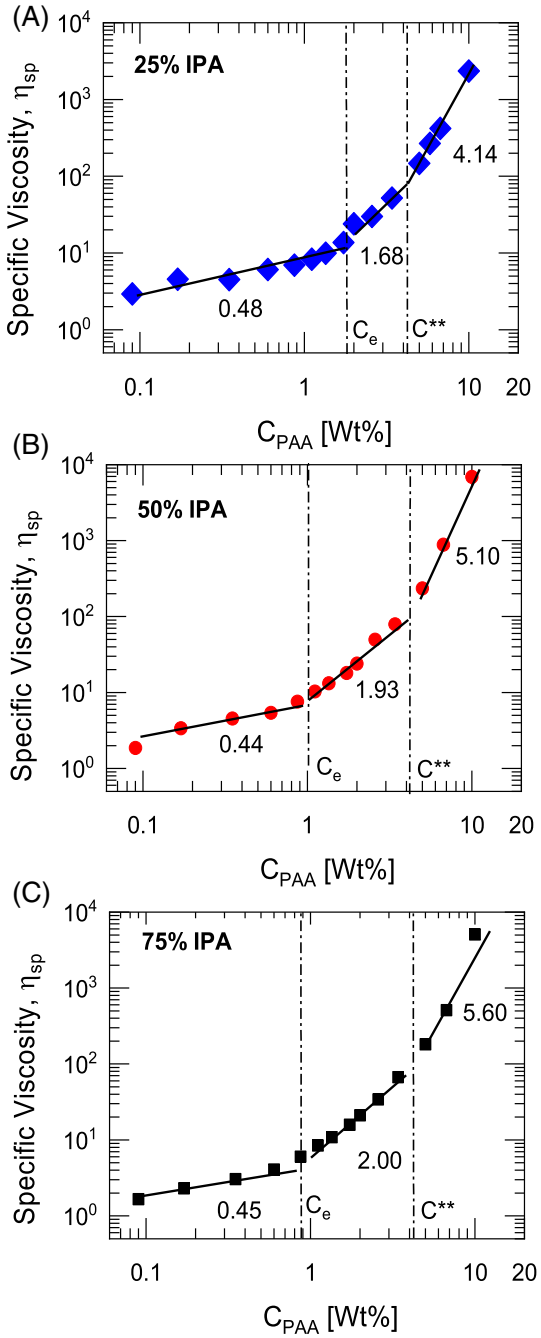

FIGURE 1 Specific viscosity $\eta_{sp} = (\eta_0 - \eta_s)/\eta_s$ versus poly(acrylic acid) concentration (C_{PAA}) for solutions at different IPA wt% in the solvent mixture: (A) 25%, (B) 50%, and (C) 75%. The dash-lines correspond to entanglement concentration C_e and critical concentration for transition to the concentrated regime C^{**}. The η_s is the solvent viscosity

solutions, scaling was found to be unaffected by glycerol.[45] Findings were similar in perfluorinated ionomer (Nafion) dispersions in water – 1-proponal (nPA) mixtures, in our own previous study, where polyelectrolyte-like scaling remained the same for all nPA% varied between 25 and 75 wt%.[60]

Such similar polyelectrolyte-like scaling indicates electrostatic interactions at dilute concentrations are not significantly affected by IPA. At dilute concentrations, the dissociation of charged of polyelectrolytes, dictated by a combination of both enthalpic and entropic effects, is known to be enhanced by entropic effects. With decreasing concentration (or dilution), an increase free volume in the media leads to an increase in the translation entropy of the counter-ions, resulting in an increase in the degree of counter-ion dissociation, and in turn leading to an increase in the magnitude of electrostatic interactions.[61,62] The comparison of their total conductivity, expressed in terms of equivalent conductivity, $\Lambda_e = (\Lambda_t - \Lambda_0)/C$, as a function of PAA concentration (Figure S1B), further support this. For all IPA%, the Λ_e increased with decreasing PAA concentration, indicating an enhancement of their dissociation, consistent with previous reports.[61,62] Therefore, the enhanced dissociation at dilute concentrations by entropic effects, despite their low dielectric constant, could be responsible for such similar scaling for all IPA%. And the discrepancy in the scaling behavior of PAA solutions in water–IPA mixtures here with former studies on PAA as well as sodium carboxy methyl cellulose (NaCMC) solutions in water–glycerol mixtures, despite IPA being less polar than glycerol, suggests that other factors (i.e., H-bonding, solubility, and hydrophobic interactions) play a role in the scaling behavior, beyond the differences in their dielectric constant.

Although scaling in the unentangled regime is insensitive to IPA%, a closer look at the data shows some variation of η_{sp} with IPA%. As shown in Figure 2A, at low concentrations (<0.18% PAA), η_{sp} decreases with increasing IPA%, by ~30%–45% between 25% and 75% IPA. Such trend suggests a decrease in size or pervaded volume with increasing IPA%. Although scaling remains polyelectrolyte-like for all IPA%, indicating an overall extended structure at dilute concentration, the trends of η_{sp} indicate some decrease in their chain size with increasing IPA%. This is likely due to a decrease in the magnitude of intra-chain electrostatic repulsions, responsible for their extended structure, due to decreasing polarity. In addition, any modification of PAA solubility by IPA could also play a role.

Next examining the behavior beyond the unentangled regime, the effect of IPA% on scaling is stronger. The entangled concentrations C_e were approximately 1.73, 1.10, and 0.87 wt% for 25%, 50%, and 75% IPA, respectively, where the value reduces by ~50% between 25% and 75% IPA. And the scaling exponent in the semi-dilute entangled (n_1) regime increases with increasing IPA%, where $n_1 \sim 1.68$, 1.93, and 2.0 for 25%, 50%, and 75% IPA, respectively. The value increasingly deviates from

26424169, 2023, 14, Downloaded from https://onlinelibrary.wiley.com/doi/10.1002/pol.20220719 by National Renewable Energy Lab, Wiley Online Library on [27/07/2023]. See the Terms and Conditions (https://onlinelibrary.wiley.com/terms-and-conditions) on Wiley Online Library for rules of use; OA articles are governed by the applicable Creative Commons License

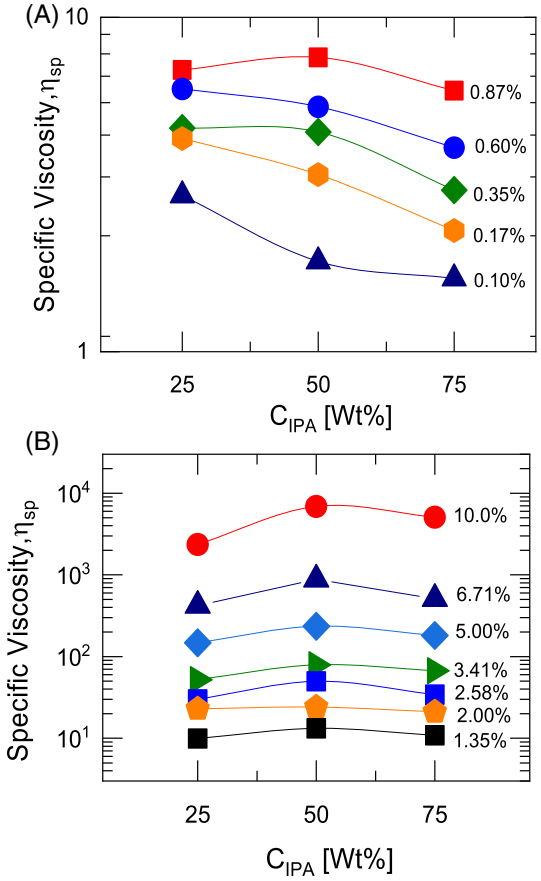

FIGURE 2 (A, B) Specific viscosity as a function of IPA% at various poly(acrylic acid) concentrations

the reported value for aqueous salt-free polyelectrolytes of $n_1 \sim 1.5$.[17,28,45,63,64] This observation also differs from NaCMC and PAA solutions in water–glycerol mixtures, where their scaling was found to be unaffected by the addition of glycerol, such that $n_1 \sim 1.6$–1.5 for both polymers.[45,46] However, a similar increase was reported by Jimenez et al.[45] for aqueous NaPSS solutions with glycerol addition from $n_1 \sim 0.85$ to 1.1, but much weaker compared to the PAA solutions here.

The scaling of the PAA solutions in the concentrated regime also similarly varies with IPA%, where the scaling exponent increases as $n_2 \sim 4.14$, 5.10, and 5.60, for 25%, 50%, and 75% IPA, respectively. And the value increasingly deviates from $n_2 \sim 3.75$ reported of aqueous salt-free polymer solutions in the concentrated regime.[17,28,63,64] Note that the scaling exponent in the concentrated regime is similar to that of neutral polymers, $n_2 \sim 3.75$. This is due to screening of electrostatic interactions at high concentrations, because as the concentration is increased, the degree of dissociation of counter-ions reduces, causing a decrease in the translation entropy of the counter-ions to dissociate due to crowding.[65] This leads to a decrease in the magnitude of electrostatic repulsions, causing them to behave like neutral polymers.[28,66] Similar large exponents have been reported for NaCMC solutions in water ($n_2 \sim 5.5$),[67] and for other aqueous polyelectrolytes solutions in the presence of salt, sodium alginate ($n_2 \sim 5.9$)[68] and xanthum gum ($n_2 \sim 4.76$).[64]

At low concentrations (unentangled regime), a decreasing trend in η_{sp} indicated a decrease in PAA size with increasing IPA%. This was attributed to decreasing intra-chain electrostatic interactions, reducing the chain extension. Whereas, in the entangled and concentrated regimes, with increase in IPA%, the scaling increased, and the C_e decreased. We observed similar trends, and much stronger, in perfluorinated ionomer dispersions in the same solvent mixture with varying IPA%, which will be discussed in our forthcoming publication. Such trends at higher concentrations, in contrast, indicate a growth in the PAA structure or an increase in PAA aggregation.

Many previous studies show salt-free aqueous polyelectrolyte solutions can aggregate at high concentrations, referred to as clustering where they form loose aggregates[69,70]; although the exact mechanisms for such occurrence has been a subject of significant research through theory,[70–73] experiments,[74–78] and simulations.[79–82] As noted before, as the concentration of polyelectrolyte is increased, the fraction of condensed counter-ions increases, (or the degree of dissociated counter-ions, conversely, decreases).[65] Such condensation is believed to play role in their clustering, where the condensed ionic groups have been proposed to induce attraction via one or more mechanisms, such as, dipolar attraction[69,71,73] and counter-ions mediated electrostatic attraction.[70,72,79–81]

The PAA solutions here could similarly aggregate above a certain concentration. In a previous SANS study on PAA solutions in various solvent systems including water–alcohol (ethanol) mixtures, Hammouda et al.[83] indeed report aggregation or clustering of PAA, both in pure solvents (water and ethanol) as well as in their mixtures, based on an upturn in the scattering intensity at low scattering vectors corresponding to larger length scales. As discussed previously, with increasing IPA%, the degree of condensation of PAA increases, leading to an increase in the magnitude of both dipolar attraction and counter-ion mediated electrostatic attractions between PAA molecules. Such increase could result in an increase in the PAA aggregation. However, additional studies are required to confirm such trend in the aggregation using techniques such as neutron scattering and cryo-transmission electron microscopy (cryo-TEM).

However, if we examine the trend of η_{sp} at higher PAA concentrations, it suggests the aggregation variation is not monotonic with IPA%. We can see in Figure 2B

26424169, 2023, 14, Downloaded from https://onlinelibrary.wiley.com/doi/10.1002/pol.20220719 by National Renewable Energy Lab, Wiley Online Library on [27/07/2023]. See the Terms and Conditions (https://onlinelibrary.wiley.com/terms-and-conditions) on Wiley Online Library for rules of use; OA articles are governed by the applicable Creative Commons License

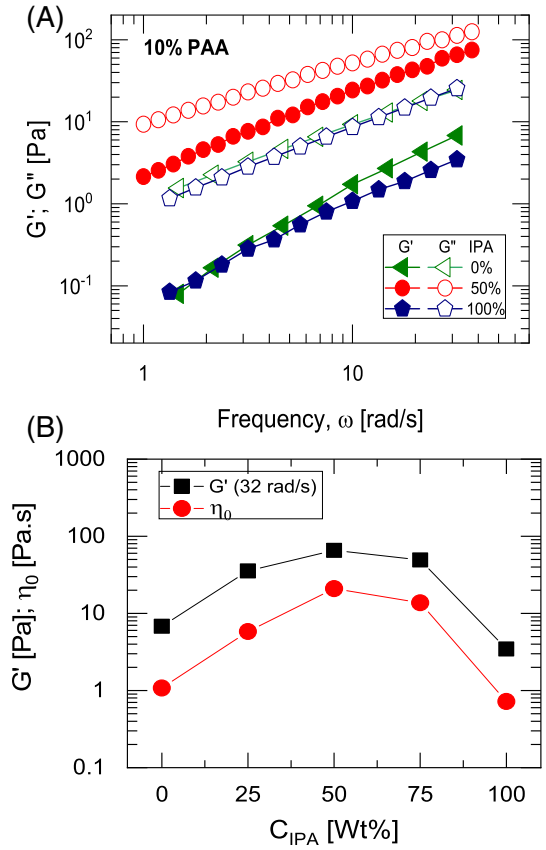

FIGURE 3 (A) Frequency sweep measurements and (B) high-frequency modulus and zero-shear viscosity as a function of IPA% (0%, 50%, 100% IPA) at a fixed poly(acrylic acid) concentration of 10 wt%

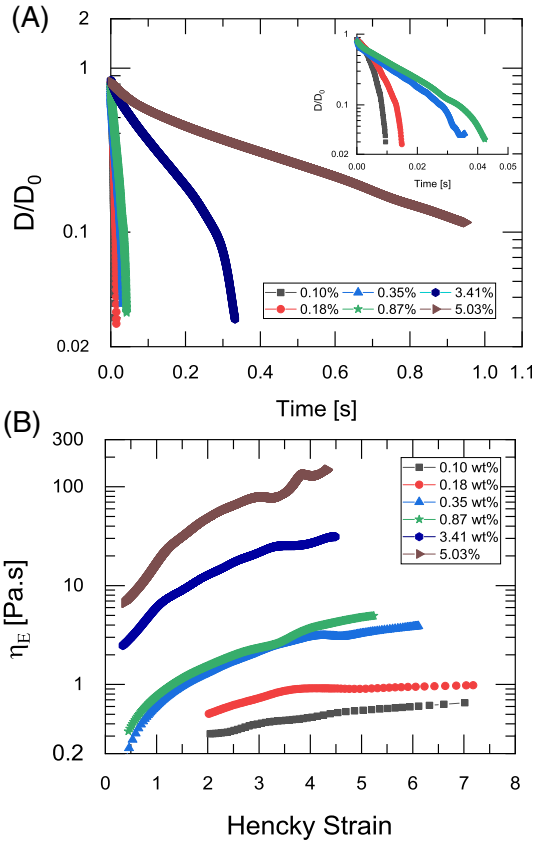

FIGURE 4 Extensional rheology data of poly(acrylic acid) (PAA) solutions at a series of PAA concentrations at 50% IPA in the solvent mixture characterized using DOS rheometry: (A) Normalized filament diameter $D(t)/D_0$ versus time and (B) Extensional viscosity η_E versus Hencky strain. The filament diameter (D) was normalized by the needle diameter (D_0). The inset in figure A shows zoom in data of low PAA concentrations

that it displays a maximum in the entangled and concentrated regimes (>0.6 wt% PAA). Such maximum in the shear viscosities suggest a maximum in PAA aggregation at 50% PAA. To further evaluate this linear viscoelasticity at a fixed PAA concentration (10 wt%), has been compared, and the tests have also been extended to pure solvent cases (0% and 100% IPA). In Figure 3A, the frequency response of only pure cases and 50% IPA cases are compared for clarity. The data of all cases, including their steady shear rheology, is provided in Figure S2; however, the data, elastic moduli (at high $\omega \sim 32$ rad/s) and zero-shear viscosity η_0, of all cases is compared in Figure 3B. The elastic moduli values show a similar trend to η_0, exhibiting a maximum at 50% IPA case. The values of 50% IPA cases are larger than for the pure solvent cases by a factor between 4 and 20. And all the solutions show a predominantly viscous response, $G' < G''$ throughout the frequency range. Furthermore, comparing the moduli scaling at low frequencies, $G' \sim \omega^{n1}$ and $G'' \sim \omega^{n2}$, all cases do not approach terminal scaling of $G' \sim \omega^2$ and $G'' \sim \omega^1$ at lowest frequencies characterized, scaling weaker with exponents ranging between $n_1 \sim 1.48$–1.09 and $n_2 \sim 0.91$–0.80. But the scaling exponents of 50% are the smallest ($n_1 \sim 1.0$ and $n_2 \sim 0.77$) compared to all cases. This suggests a maximum relaxation time of the solution, and thus the elasticity at 50% IPA. These comparisons further indicate maximum aggregation at intermediate alcohol fraction.

Such trends have been previously reported for PAA in water-ethanol mixtures, as well for NaCMC in water–glycerol mixtures, and also commonly observed in pure binary water–alcohol mixtures.[3,34,45] Neutral polymers were also found to show a similar non-monotonic trend in water–alcohol mixtures.[84–86] Studies on pure solvent mixtures suggest such maximum arises from orientation/restructuring of water around solvent to maximize H-bonding.[87–89] Previous studies on polymer solutions, both neutral and polyelectrolytes, have related the non-monotonic trend in their viscosities to similar origins; though neutral polymers were found to exhibit a minimum in their viscosity, in contrast to polyelectrolytes.[84–86]

26424169, 2023, 14, Downloaded from https://onlinelibrary.wiley.com/doi/10.1002/pol.20220719 by National Renewable Energy Lab, Wiley Online Library on [27/07/2023]. See the Terms and Conditions (https://onlinelibrary.wiley.com/terms-and-conditions) on Wiley Online Library for rules of use; OA articles are governed by the applicable Creative Commons License

TABLE 1 Extensional relaxation times λ_E of the poly(acrylic acid) solutions at a series of concentrations and different IPA wt% in the solvent mixture

IPA wt%	PAA wt%	Extensional relaxation time λ_E [ms]	Elasto-capillary number Ec	Intrinsic Deborah number De_0
50%	0.10	0.5	8.10	0.90
	0.18	1.5	19.7	2.7
	0.35	3.0	19.1	5.0
	0.87	5.0	27.2	9.0
	2.00	11	17.3	22.4
	2.60	17	13.1	31.7
	3.41	48	26.2	86.0
	5.03	180	32.3	322
25%	2.00	7	15.4	13.5
	2.60	14	26.2	28.6
75%	2.00	13	24.7	27.2
	2.60	20	23.6	37.0

Note: The evaluated dimensionless numbers are also shown, which include the Elasto-capillary number Ec and the Intrinsic Deborah number De_0.

However, owing to the presence of charged groups, the viscoelasticity enhancement at intermediate alcohol fractions in polyelectrolytes can be expected to be dictated by the interplay of multiple interactions, such as electrostatic and dipolar interactions, in addition to H-bonding and polymer solubility.[34] In a previous study by Vats et al.[34] on PAA in water–ethanol mixtures, the viscosity maximum has been proposed to arise from maximum expansion of the PAA coil at those conditions. However, the comparisons here at a wider concentration range, including the unentangled regime, as well as addition measures—the elasticity and the η_{sp} scaling—as discussed above, suggest the role of PAA aggregation in the viscosity maximum. Further confirmation of their structure, both in the dilute and non-dilute regime, will provide more insights into the origins of the viscoelasticity enhancement at intermediate alcohol fractions.

3.1.2 | Extensional rheology

The extensional rheological properties of the PAA solutions as a function of PAA concentration at fixed IPA% are first discussed. The diameter decay data for a series of PAA concentrations at 50% IPA characterized using DOS-rheometry are compared in Figure 4A. All solutions decay like viscoelastic fluids, that is, a linear decay initially, followed by an exponential decay.[90] The ratio of elastic and viscous stresses is given by the dimensionless Weissenberg number, Wi. Above the critical Weissenberg number $Wi_c = 0.5$, the elastic effects become important due to coil-to-stretch transition of the polymers.[91] Therefore, the observed transition from a linear to the exponential decay marks the onset of elastic effects where $Wi > Wi_c \sim 0.5$. The extensional relaxation times λ_E determined from the diameter decay data using the equations outlined in section 2.3 are summarized in Table 1. As shown in Figure 5A, the extensional relaxation time increases with increasing PAA concentration, consistent with previous studies.[36,55,92]

The Zimm relaxation time (λ_Z), which is a lower bound for relaxation time of polymer solutions, has also been evaluated to validate the measurements. This is given by $\lambda_Z = \Lambda[\eta]\eta_s M_w/RT$, where R is the gas constant (8.316 J K^{-1} mol^{-1}), T is the temperature. The $\Lambda = 1/\zeta(3\upsilon)$ is a pre-factor, depends on the solvent quality exponent υ, which varies between 0.42 and 0.55, and ζ is a Riemann zeta function. The intrinsic viscosity $[\eta] \sim$ 2.42 dL/g was obtained by fitting the data to Fedors equation[93,94] previously used for unentangled polyelectrolyte solutions as discussed in Figure S3. The value is smaller than reported for PAA solutions in water ($[\eta]_w \sim 20$ dL/g) and glycerol–water mixture 70/30 ($[\eta]_{w/g} \sim 5$ dL/g) of similar M_w, consistent with the relatively low polarity of the 50% IPA solvent mixture. And using solvent viscosity $\eta_s \sim 2.2$ mPa s, $M_w \sim 450$ kg/mol, temperature $T = 298$ K, and $\Lambda \sim 0.42$ (assuming a theta condition), we obtain $\lambda_z \sim 0.06$ ms. The extensional relaxation time of all the solutions measured are larger than the λ_z, which is shown as a dotted line in Figure 5A. The lowest measured relaxation time (corresponding to 0.1 wt% PAA) is at least 8x larger than λ_z. This is expected, as the

26424169, 2023, 14, Downloaded from https://onlinelibrary.wiley.com/doi/10.1002/pol.20220719 by National Renewable Energy Lab, Wiley Online Library on [27/07/2023]. See the Terms and Conditions (https://onlinelibrary.wiley.com/terms-and-conditions) on Wiley Online Library for rules of use; OA articles are governed by the applicable Creative Commons License

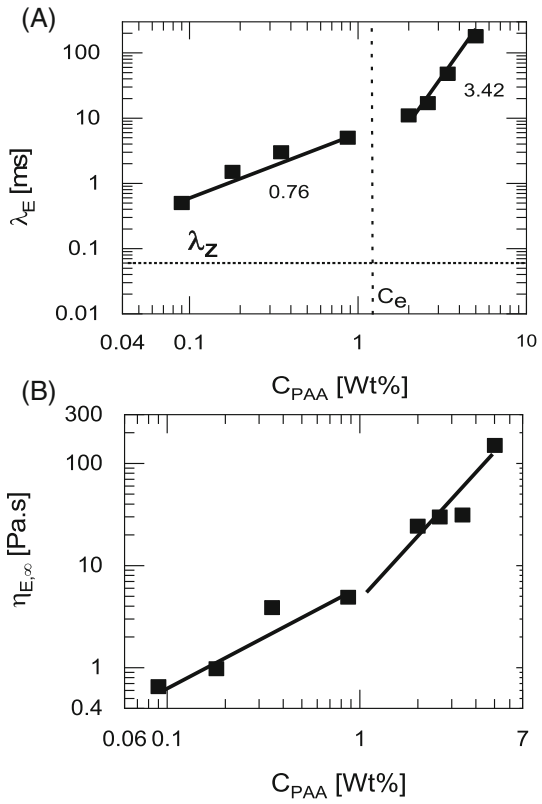

FIGURE 5 (A) Extensional relaxation time and (B) maximum extensional viscosity, $\eta_{E,\infty}$, as a function of poly(acrylic acid) (PAA) solutions at 50% IPA in the solvent mixture. The dotted line in figure a corresponds to the estimated Zimm relaxation, $\lambda_Z \sim 0.06$ ms

PAA concentrations here are much larger than dilute or ultra-dilute concentrations where the extensional relaxation times are expected to approach λ_Z.[23]

Examining the scaling in the semi-dilute unentangled regime, we observe $\lambda_{E\sim}C^{0.76}$ (Figure 5A). For neutral flexible polymer solutions (aqueous solutions of polyethylene oxide [PEO]), the extensional relaxation time was found to scale as $\lambda_{E\sim}C^{1}$.[95,96] Whereas for PAA solutions in water, Jimenez et al. found a weaker scaling, $\lambda_{E\sim}C^{0.5}$.[45] For stronger polyelectrolytes, NaPSS, they reported the relaxation times in unentangled regime to be too low to measure in both water and water-glycerol mixture, and determine the scaling behavior. The deviations from neutral flexible polymers have been proposed to mainly arise from their partially or fully extended equilibrium conformation in solution owing to intrachain electrostatic repulsions. This would lead to a partial or lack of coil-stretch transition in extensional flow, resulting such weaker scaling or small λ_E values, unlike in the case of flexible neutral polymers where the coils can be fully extended.[45]

The scaling of PAA solutions in IPA–water mixtures here is stronger compared to in water, but still weaker than neutral polymer solutions. Multiple explanations may be plausible for such deviation. The comparisons above of their shear rheology measures (η_{sp} and $[\eta]$) at low concentrations indicated that the addition of IPA leads a less extended or more compact conformation of PAA. This was attributed to a reduction in the magnitude of intra-chain electrostatic repulsions, in addition any modification of the solubility by IPA. Such compact/less-extended conformation at equilibrium, can increase their extensibility—or the degree to which chain can be extended in extension flow—and lead to a stronger scaling. Alternatively, the trends at higher concentrations—the C_e, as well as that of the scaling exponent and the magnitude of η_{sp} as a function of IPA%—indicated attractive interactions between PAA and their tendency to aggregate. And, unlike in shear, the stretching effect in extensional flow is known to increase the interchain interactions between polymer coils, even in the dilute regime.[23] Because of the attractive interactions between PAA, the enhanced interchain interactions in extension flow could induce aggregation/structure buildup of PAA, and stabilize the filaments. Such flow-mediated aggregation of PAA in extensional flow could also result in a stronger λ_E scaling. The exact mechanism however needs further investigation. This observation, however, deviates from previous findings on water–glycerol mixtures for both PAA and NaCMC solutions. In contrast to IPA, the scaling of both was found to be unaffected by the addition of glycerol.[45,46] They have argued such insensitivity of λ_E scaling in extension unlike in shear is due to a similar stretched/elongated conformation in extensional flow where the intra-chain interactions—electrostatic, hydrodynamic, and excluded volume interactions—are screened.[45] The deviation could be attributed to differences in the effects between IPA and glycerol on the chain conformation and interchain interactions. This is evident based on the differences in the η_{sp} scaling behavior in both unentangled and entangled regime as well as the $[\eta]$, as discussed above.

If we next examine the scaling in the entangled regime, the scaling exponent of the PAA solutions here is similarly larger, $n \sim 3.42$, compared to previous reports on PAA solutions in water, where $n \sim 1.5$, as well as aqueous NaCMC solutions, where $n \sim 1.0$–1.1.[45,46] Such larger scaling also deviates from previous findings on glycerol-water mixture for both PAA and NaCMC solutions, where the scaling to be similar that of in water. The stronger scaling of the PAA solutions could similarly be attributed to flow-mediated increase in PAA aggregation in water-IPA mixtures, in addition to the contribution from chain entanglements that become important in the entangled regime. Similar stronger scaling exponents have also been reported for aqueous 2-hydroxyethyl

26424169, 2023, 14, Downloaded from https://onlinelibrary.wiley.com/doi/10.1002/pol.20220719 by National Renewable Energy Lab, Wiley Online Library on [27/07/2023]. See the Terms and Conditions (https://onlinelibrary.wiley.com/terms-and-conditions) on Wiley Online Library for rules of use; OA articles are governed by the applicable Creative Commons License

cellulose (HEC) solutions ($n \sim 4.3$)[97] and cellulose solutions in ionic liquids ($n \sim 3.8$).[98]

Extensional viscosity as function of Hencky strain for all PAA concentrations are shown in Figure 5B. All solutions show strain-hardening due to the onset of elastic effects, as evidenced from the exponential diameter decay profiles. And the extensional viscosities at large strains, $\eta_{E,max}$, increases with increasing PAA concentration (Figure 5B). And their scaling in the semi-dilute entangled regime, $c > 1.10$, is stronger compared to in the semi-dilute unentangled regime due to a combination of chain entanglements and PAA aggregation. The ratio of extensional and shear viscosity, given by Trouton ratio $Tr = \eta_E/\eta_0$, has been compared (Table 1). For simple Newtonian fluids, $Tr = 3$, whereas for viscoelastic polymer solutions, $Tr >> 3$ due to the coil-stretch effect in extensional flow fields.[55,99] For the PAA solutions here, the maximum Trouton ratio (or Tr at large strains) is $87 < Tr_{max} < 680$ for all concentrations, which is ~30–220 × larger than for a simple Newtonian liquid due to strain hardening.

The extensional rheology of PAA solutions at other IPA% (25% and 75%) was characterized at a few representative PAA concentrations. The diameter decay data of different IPA%, including 50% IPA, at 2% and 2.6 wt% PAA concentrations, characterized using CaBER was compared in Figure 6A,B, respectively. The filament decay profiles of all cases are similar to viscoelastic fluids, as discussed previously. The extensional relaxation times were compared as a function of IPA% in Figure 6C. Given that the extensional relaxation time also increases with the solvent viscosity, the values were normalized by the solvent viscosity ($\lambda_N = \lambda_E/\eta_s$) to better capture differences due to the polymer contribution. For both concentrations, λ_N overall increases with increasing IPA%. This suggests an increase in the elasticity of the PAA solutions with increasing IPA%, resulting an enhancement in the stability of their filaments in extensional flows, such as electrospinning, against capillary break-up.

Such monotonic trend in λ_N, however, differs from the shear measures, both η_{sp} (as coplotted at the same concentrations) and the moduli values (Figure 3B) characterized at higher PAA concentrations, which in contrast exhibit a maximum at 50% IPA. We have attributed the trends of shear flow properties predominantly to the variation of their aggregation. The discrepancy at high IPA% between shear and extensional flow suggests that other mechanisms may be dominating their extension flow response at high IPA%. Similar deviations in the trends between shear and extensional flow measures as a function of alcohol cosolvent have been previously reported. Kheirandish et al.[44] who studied alkali-swellable acrylic thickeners in water–ethanol mixtures,

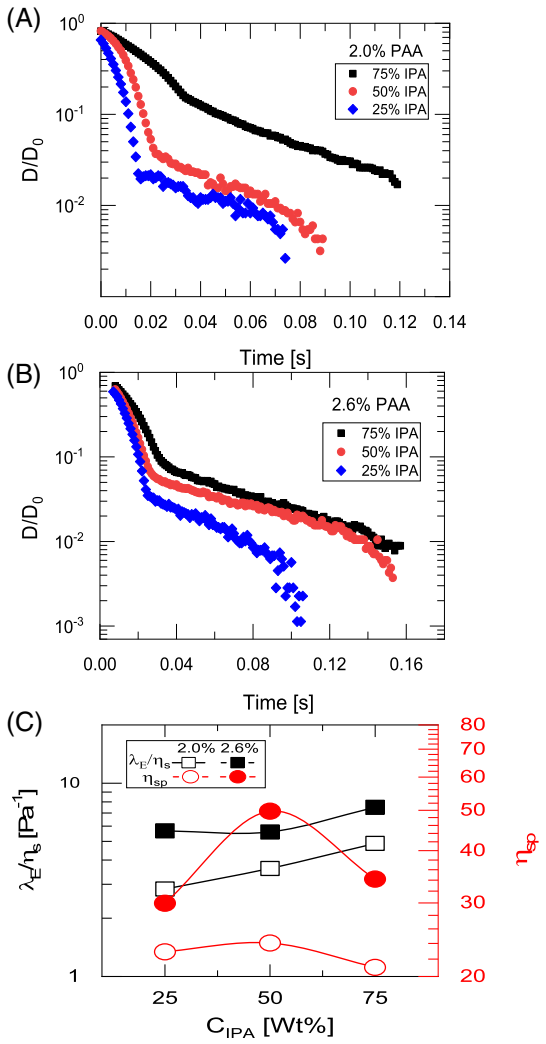

FIGURE 6 Extensional rheology data of poly(acrylic acid) (PAA) solutions at different IPA% in the solvent-mixture characterized using CaBER. The data include PAA concentrations of (A) 2.0 wt% and (B) 2.6 wt%. The filament diameter (D) was normalized by the needle diameter (D_0). (C) Extensional relaxation time (normalized by the solvent viscosity) λ_E/η_s (left axis, data in square symbols) and specific viscosity η_{sp} (right axis, data in circle symbols) as a function of IPA% for 2% and 2.6% PAA concentrations

consisting of hydrophobic groups that associate in water, found that with increasing ethanol fraction, both shear viscosities and shear relaxation times exhibited a maximum. The extensional relaxation times, in contrast, were found to monotonically increase. This has been attributed to a decrease in the hydrophobic aggregation as result of an increase in the solvent quality with the hydrophobic groups, allowing an extension of more free chains in flow, leading to the increase in the relaxation times. The mechanism of the enhancement of extensional relaxation time at high IPA% here could be different. Better understanding of the variation of PAA structure by IPA% and

26424169, 2023, 14, Downloaded from https://onlinelibrary.wiley.com/doi/10.1002/pol.20220719 by National Renewable Energy Lab, Wiley Online Library on [27/07/2023]. See the Terms and Conditions (https://onlinelibrary.wiley.com/terms-and-conditions) on Wiley Online Library for rules of use; OA articles are governed by the applicable Creative Commons License

Sample	Primarily beads	Onset of beaded fibers		Onset of uniform fibers	
	C_b [wt%]	C_{fb} [wt%]	C_{fb}/C_e	C_f [wt%]	C_f/C_e
25% IPA	≤0.35	0.60	0.35	3.41	1.97
50% IPA	≤0.18	0.35	0.32	2.60	2.36
75% IPA	≤0.18	0.35	0.40	1.71	1.96

TABLE 2 Critical poly(acrylic acid) concentration for the formation of different fiber morphologies which include predominantly beads C_b, beaded fibers C_{fb}, and uniform (beads-free) fibers C_f, and their ratios with entanglement concentrations (C_{fb}/C_e and C_f/C_e) at different IPA% in the solvent mixture

the underlying interaction mechanisms is required to explain this discrepancy.

The deviations in their scaling of their extensional relaxation time compared to PAA solutions in aqueous media, as well as the distinct trend of their extension relaxation time from shear rheology measures as a function of IPA%, suggest complex interplay of multiple interactions are controlling their structure, and in turn affecting their shear and extensional flow response differently based on the IPA fraction in the solvent-mixture.

3.2 | Electrospinning

3.2.1 | Fiber morphology

Electrospinning experiments were conducted on PAA solutions for a series of concentrations (0.18–3.41 wt%) and at different IPA%. Table 2 summarizes the morphologies obtained at different PAA concentrations. The SEM images of the fiber morphologies at representative PAA concentrations are shown in Figure 7. For all IPA %, with increasing PAA concentration, the morphologies progressively transform from predominantly beads, like an electrospraying process (images A, E, and I), to beaded fibers (images B and C, F and G, and J and K), and then to uniform fibers (images D, H, and L). This progression is consistent with previous findings on polymer solutions.[12,26,66] As shown in Figure S5, the fiber diameter, characterized at a few representative concentrations, also increases with increasing PAA concentration. Between 2 and 3.41 wt% PAA, the mean fiber diameter of 25%, 50%, and 75% IPA cases increases from 73 to 312 nm, 165 to 357 nm, and 85 to 271 nm, respectively. And the smallest uniform fiber obtained here has a mean diameter of 62 ± 16 nm, and corresponds to 2.6 wt% PAA in 75% IPA solutions. The overall improvement in the fiber uniformity as well as the increase in the fiber diameter is qualitatively consistent with changes in the viscoelasticity of solutions, which increases with increasing PAA concentration, that would promote the stability of the jet against break-up, or resisting the thinning of the jet by inertia.

However, comparing between different IPA%, the critical concentration for the onset of both beaded fibers (C_{fb}) as well as uniform fibers (C_f) varies with IPA%. As shown in Figure 8A, the C_{fb} decreases with increasing IPA%: $C_{fb} \sim 0.60$ wt% for 25% IPA, and $C_{fb} \sim 0.35$ wt% for both 50% and 75% IPA. The onset of uniform fibers C_f similarly decreases with increasing IPA%, where $C_f \sim 3.41\%$, 2.60%, and 1.71% for 25%, 50%, and 75% IPA, respectively, where it reduces by ~50% between 25% and 75% IPA. The overall improvement in the fiber uniformity with increasing alcohol content is in agreement with previous reports on PAA solutions in water–ethanol mixtures[3,34] as well as neutral polymers.[40,43]

As noted before, the addition of alcohol influences several solution properties, such as interfacial tension, conductivity, and volatility, including their rheology, which are also known to impact the fiber morphologies. We first examine the correlation between rheological properties and the fiber formation. Both an increase in the elasticity or viscosity of the fluid is known to facilitate fiber formation. The comparison of the shear rheology between different IPA% showed that the trend of their shear viscosities varies depending on the concentration range. In the unentangled regime they decrease with increasing IPA%; whereas in both the entangled and concentrated regime, they vary non-monotonically, displaying a maximum at 50% IPA. Their extensional rheology in contrast, compared in the entangled regime, varies monotonically with IPA%, where the extensional relaxation time increases with increasing IPA%. If we qualitatively compare the trends between shear (η_0) and extensional flow properties (λ_E) against that of the onset of fiber formation (C_{fb} and C_f) as a function of IPA%, we can see a better correspondence between extensional rheological properties and the fiber formation, compared to shear rheology. The decreasing trend of both C_{fb} and C_f with increasing IPA% is consistent with the increasing trend of the λ_E. Such correspondence suggests that an increase in elasticity is likely promoting their fiber formation.

We further analyze the relative importance of elastic and viscous forces on the initial jet dynamics by evaluating the Elasto-Capillary Number, a global dimensionless number that compares the magnitude of elastic forces and

26424169, 2023, 14, Downloaded from https://onlinelibrary.wiley.com/doi/10.1002/pol.20220719 by National Renewable Energy Lab, Wiley Online Library on [27/07/2023]. See the Terms and Conditions (https://onlinelibrary.wiley.com/terms-and-conditions) on Wiley Online Library for rules of use; OA articles are governed by the applicable Creative Commons License

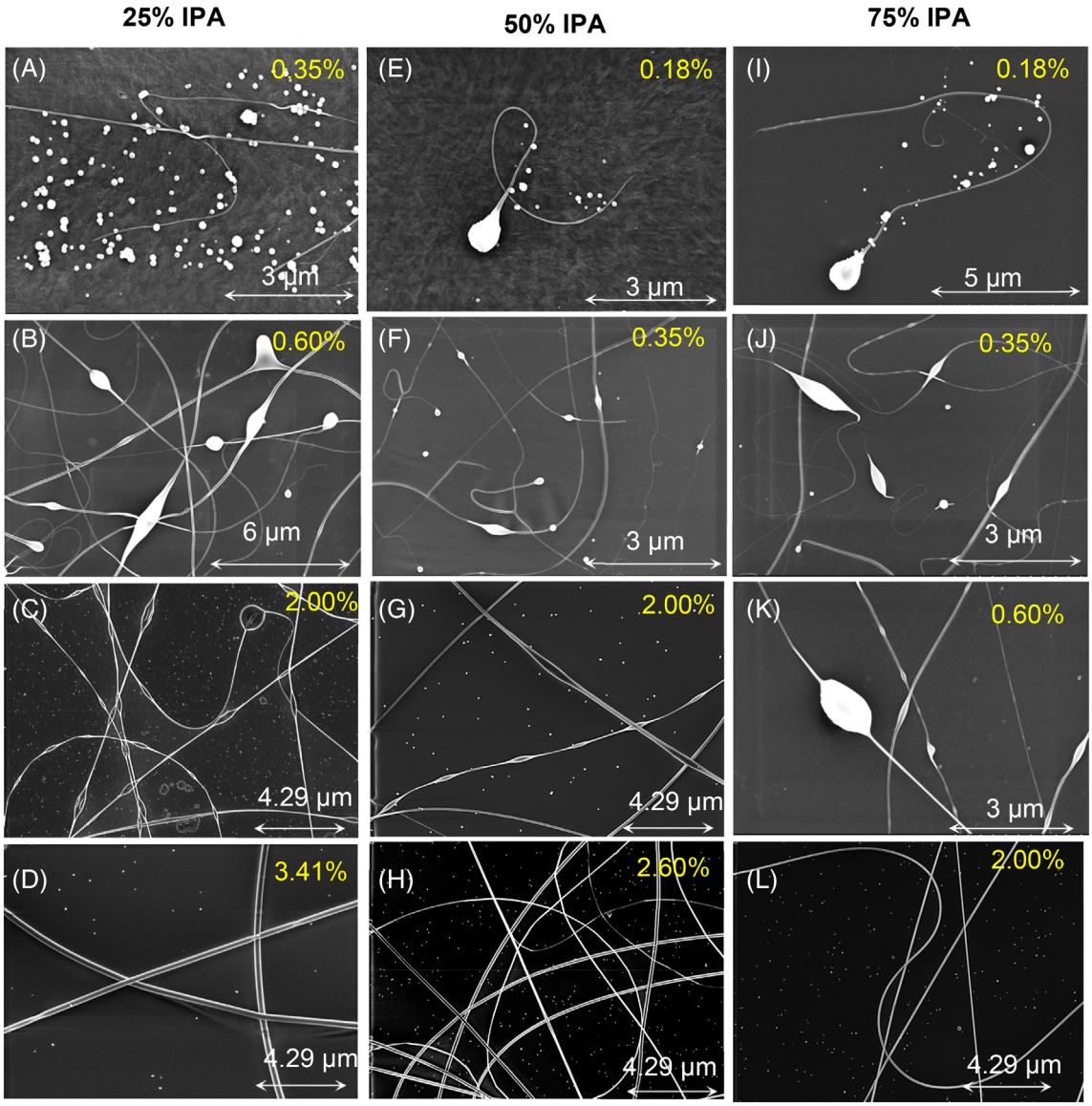

FIGURE 7 Scanning electron microscope images of fiber morphologies at a series of poly(acrylic acid) concentrations with different IPA wt% in the solvent-mixture: 25% IPA (A–D), 50% IPA (E–H), and 75% IPA (I–L)

viscous forces. This is defined as $Ec \sim \lambda_E \sigma / \eta_0 R_0$, where R_0 is the radius of the nozzle, which is taken as the characteristic length scale of the process. Elastic forces dominate viscous forces when $Ec > Ec_c \sim 4.7$.[100] The evaluated Ec values are compared in the Table 1. For all PAA concentrations and IPA%, Ec >4.7. This suggests that solutions are predominantly elastic, and elastic forces would dominate the jet dynamics, rather viscous forces, and thus the fiber formation. This further supports a better correlation between extensional relaxation rheology, over shear, and the fiber formation. Comparison of the corresponding shear viscosities, in terms of dimensionless Ohnesorge number Oh, and the onset of fiber formation also shows no clear correlation. The Oh is defined as the ratio of viscous and inertia, given by $Oh = \eta_0 / \sqrt{\rho \sigma R_0}$. The Oh corresponding to the onset of fiber formation are very close similar $Oh_{fb} \sim 0.26$–0.18, and also close to $Oh_c \sim 0.2$,[71] where viscous forces are shown to dominate inertia. However, if we compare the corresponding viscosity values, they decrease with increasing IPA% (by ~38% between 25% and 75% IPA), and thus do not correlate with the onset of the fiber formation. The observations are similar for comparisons at the onset of uniform fiber formation, although Oh_f values differ significantly, by a factor of 3, between different IPA% where $Oh_f \sim 1.87$, 2.42, and 0.74 for 25%, 50%, and 75% IPA, respectively. And the corresponding shear viscosities similarly decrease with increasing IPA%.

Analogous to the Oh, the relative importance of elastic forces over inertia is given by the intrinsic Deborah number $De_0 \sim \sqrt{\lambda_E^2 \sigma / \rho R_0^3}$, where ρ is the fluid density. The elastic forces are shown to dominate inertia when $De_0 > De_{0c} \sim 1$.[100] Note however that for the onset of

26424169, 2023, 14, Downloaded from https://onlinelibrary.wiley.com/doi/10.1002/pol.20220719 by National Renewable Energy Lab, Wiley Online Library on [27/07/2023]. See the Terms and Conditions (https://onlinelibrary.wiley.com/terms-and-conditions) on Wiley Online Library for rules of use; OA articles are governed by the applicable Creative Commons License

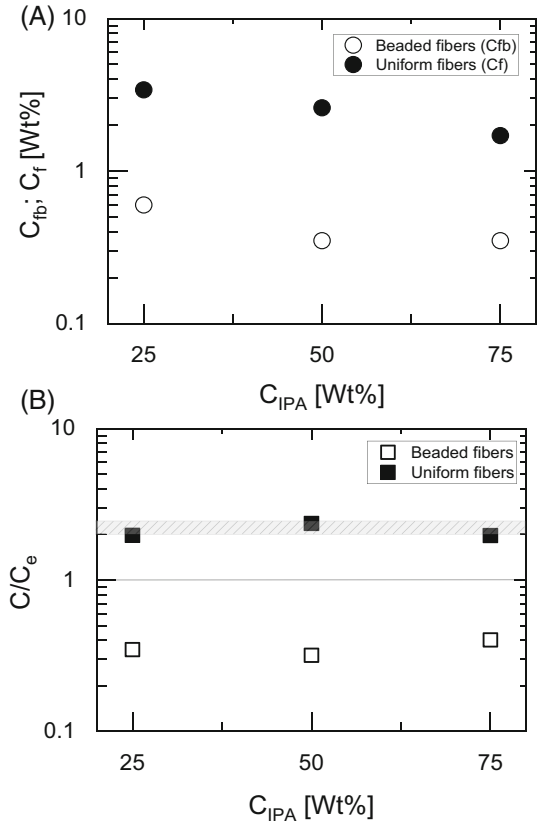

FIGURE 8 Plots of (A) critical poly(acrylic acid) concentration for the onset of fiber formation (beaded-fibers, C_{fb}) and uniform fibers (fibers only, C_f) and (B) their ratios with entanglement concentration (C_e) for different IPA% in the solvent-mixture. The solid line and shaded region in Figure 6B correspond to the onset of fiber formation $C_{fb}/C_e \sim 1$ (beaded fibers) and the onset of uniform fibers $C_f/C_e \sim 2$–2.5, respectively, reported for neutral polymers.

elastic effects, the Weissenberg number of the flow must exceed $Wi_c \sim 0.5$. This is likely in electrospinning, because the extension rates experienced by jets during electrospinning are known to be typically very large.[101]

Unlike Oh, the extensional rheology was characterized only at limited PAA concentrations for 50% and 75% IPA cases, (which were mostly beyond the onset of beaded fibers and span limited morphologies) to make a direct comparison and confirm the correlation between elasticity and fiber morphology. Figure 9 compares De_0 between different IPA% as a function of normalized PAA concentration (by the respective C_e). For the 50% IPA data, the Deborah numbers corresponding to beads-only morphology, beaded-fibers, and uniform fibers are $De_{0,b} < 5$, $De_{0,fb} \sim 5$–22, and $De_{0,f} > 25$, respectively. For 25% IPA, $De_{0,fb} \sim 13.5$–28.6, and for 75% IPA $De_{0,f} \sim 27$–37, falling within or close to a similar range as 50% IPA cases. Examining the data of all IPA% together shows a good correlation between De_0 and fiber morphologies, where the fiber uniformity improves with increasing De_0, in contrast to Oh. Overall, the onset of the beaded fibers and uniform fibers correspond to $De_{fb} \geq 5$ and $De_f > 22$, respectively.

Note however the De values are ~2–5 × larger compared to the previous reports on neutral polymers. Yu et al.[14] have reported $De_{fb} \geq 1$ and $De_f \geq 6$ for the onset of beaded and uniform fibers, respectively, for aqueous PEO solutions. Ewald et al.[102] have reported $De \sim 2$ for the onset of beaded fibers and $De \sim 4.5$ for the onset of uniform fibers for both aqueous PEO and PVA (polyvinyl alcohol) solutions, which are close to that of Yu et al. Though further investigation may be needed to explain this discrepancy, it is likely due to differences in the polymer type between our study and the previous studies, that is, polyelectrolytes versus neutral polymers. In the stretching regime of the jet evolution process during electrospinning, polymers are presumed to approach infinite steady-state extensional viscosity $\eta_{E,\infty}$ which predominantly dictate the late-stage dynamics of the jet, and thus the fiber formation.[22] Due to the extended rod-like structure of polyelectrolytes which reduces their extensibility, their $\eta_{E,\infty}$ is known to be lower compared to neutral polymers.[92] These differences would influence the late-stage jet dynamics, and are likely not captured by the global dimensionless numbers that mainly predict the initial jet dynamics, and therefore the discrepancy.

3.2.2 | Comparison between the onset of fiber formation and the entanglement concentration

As discussed in the introduction, previous studies on polyelectrolytes have reported the onset of beaded fibers and uniform fibers to be larger compared to neutral polymers where $C_{fb} \sim 2.5$–$7 \times C_e$, and $C_f \sim 8 \times C_e$ or larger.[17–21] From a similar comparison here, the onset of beaded fibers and uniform fibers are $C_{fb} \sim 0.3$–$0.4 \times C_e$ and $C_f \sim 2$–$2.36 \times C_e$, respectively, for all IPA% (Figure 8B). These are much lower compared to the previous reports on salt-free polyelectrolyte solutions. The deviation is likely due to the differences in the molecular weights between the studies. The molecular weight of PAA here is $M_w \sim 450{,}000$ g/mol, which is larger compared to most of the previous studies which ranged between $M_w \sim 15{,}000$ and 100,000 g/mol.[17–20] At low-molecular weights, viscous forces are expected to predominantly control the fiber formation. This is supported by the spinnability experiments of McKee et al.[66] on cationic polyelectrolyte solutions, where with screening of the electrostatic interactions by the addition of sufficient amount of salt, the onset of fiber formation was found to reduce from $C_f \sim 7 \times C_{fb}$ at a salt-free condition to

26424169, 2023, 14, Downloaded from https://onlinelibrary.wiley.com/doi/10.1002/pol.20220719 by National Renewable Energy Lab, Wiley Online Library on [27/07/2023]. See the Terms and Conditions (https://onlinelibrary.wiley.com/terms-and-conditions) on Wiley Online Library for rules of use; OA articles are governed by the applicable Creative Commons License

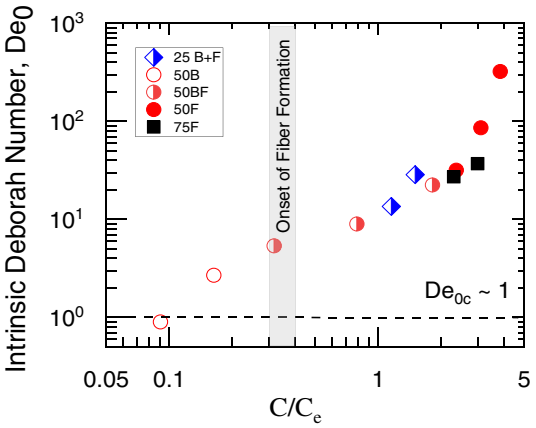

FIGURE 9 Intrinsic Deborah number De_0 as function of poly(acrylic acid) (PAA) concentration normalized by the entanglement concentration (C/C_e) for different IPA% wt% in the solvent mixture. The open, half-open, and closed symbols correspond to predominantly beads (B), beaded fibers (B + F), and unfirm fibers (F). The dashed C/C_e region correspond to the observed onset of fiber formation for the PAA solutions

$C_f \sim C_e$, approaching that of low-molecular weight neutral polymers, where viscous forces have been shown to predominantly control the fiber formation.[12,16]

Previous studies show for high-molecular weight polymers,[14,16,22,103] or high extensibility average molecular weight[104] as introduced by Palangetic et al.[16] in case of polydisperse polymers consisting a small amount of very high-molecular weight polymer, the elastic forces become more important than viscous forces, leading to a deviation in the onset of fiber formation from C_e where $C_f < C_e$, as discussed previously. Similar deviation for PAA solutions here suggests elastic effects likely dominate the jet dynamics and fiber formation. An elasto-capillary number of $Ec > Ec_c \sim 4.7$ for the solutions here, which was evaluated as discussed earlier, also supports this. Therefore, the discrepancy with the previous studies could be attributed to the predominantly elastic nature of the PAA solutions in the study, where the enhancement of the jet stability by the elastic effects is resulting a reduction in the onset of the fiber formation.

However, in the study by Subramanian et al.,[21] the molecular weight of the sulfonated polystyrene solutions, $M_w \sim 500{,}000$ g/mol, is higher than that of this work. Nonetheless, the onset of beaded fibers $C_{fb} \sim 2.6 \times C_e$ and the onset of uniform fibers $C_f \sim 3.5 \times C_e$ were larger compared to this study. This discrepancy is likely to due to differences in the molecular structure of the polymer between the studies. Polystyrene is stiffer compared to PAA. This would reduce their finite extensibility limit, and consequently the $\eta_{E,\infty}$ of the solutions,[23,45,97] increasing the concentrations required for fiber (beaded and uniform) formation.

These comparisons between the onset of fiber formation with the entanglement concentration further support the predictions of the dimensionless numbers that elastic effects predominantly control the fiber formation of the PAA solutions here. The results show that onset for fiber formation relative to the entanglement concentration of polyelectrolyte solutions, which are often larger compared to neutral polymers, could be significantly reduced by increasing the molecular weights.

3.2.3 | Other factors

Lastly, we consider the influence of other solution properties – conductivity, interfacial tension, and volatility – that also vary with IPA%, which are known to impact the fiber formation. The conductivity of the solutions decreases with increasing IPA%, as discussed earlier (Figure S1A). Particularly at concentrations near where beaded and uniform fibers are formed, their values reduce by at least 10–30 × between 25% and 75% IPA. As discussed in the introduction, very high conductivities in polyelectrolytes can adversely affect fiber formation due to large deformation rates induced by strong electrostatic repulsions that can destabilize the jet.[66] Therefore, the improvement in the fiber formation with increasing IPA% could also arise from the decrease in the solution conductivities.[66] However, the conductivities of the solutions here are several orders of magnitude smaller (on order of 10–100 $\mu S/cm^{-1}$) compared to the previous studies (which are on order of tens of mS/cm^{-1}).[66] This would result in significantly reduced jet deformation rates compared to the previous studies. Furthermore, the PAA solutions here are predominantly elastic compared to the previous studies, which can significantly hinder the jet deformation induced by the electrostatic forces. In fact, studies on highly elastic polymer solutions have found that increasing conductivities improve the fiber formation due to an increase in the degree of both strain hardening and extensional thickening with increasing jet deformation rates.[22] Therefore, the variation in the fiber formation here is likely to be dominated by the differences in the extent of buildup of extensional viscosities rather than their conductivity. To confirm this, further visualization of the jet evolution during electrospinning and the comparison of the extension rates experienced by the jet may be required.

The interfacial tension of the solvent-mixtures reduces with increasing IPA, where $\sigma = 28.9$, 24.8, and 22.5 mN/m for 25%, 50%, and 75% IPA respectively.[56] Decreasing the surface tension reduces the capillary pressure across the jet, delaying the jet break and, consequently, promoting fiber formation. However, the surface tension variation between the fluids (~22%). And the differences in their

26424169, 2023, 14, Downloaded from https://onlinelibrary.wiley.com/doi/10.1002/pol.20220719 by National Renewable Energy Lab, Wiley Online Library on [27/07/2023]. See the Terms and Conditions (https://onlinelibrary.wiley.com/terms-and-conditions) on Wiley Online Library for rules of use; OA articles are governed by the applicable Creative Commons License

surface tension were accounted for in the comparisons above against viscoelastic forces using the Oh and De_0 numbers. Lastly, the volatility of the solvent mixture increases with increasing IPA%, as the partial vapor pressure of IPA (6 kPa) is almost 2x that of water (3 kPa). This would result in an increase in the evaporation rate of the solvent and faster solidification/viscosification of the jet, increasing the jet stability. This could also promote the fiber formation.[3,40,43,105] However, a more detailed investigation into the role of differences in their drying rates on the improvement of the fiber morphologies with increasing IPA% is needed.

4 | CONCLUSIONS

We investigated the effect of isopropanol cosolvent fraction in the solvent on the rheological properties—both shear and extensional—as well as the spinnability of PAA solutions. Their specific viscosities at low concentrations decrease with increasing IPA, suggesting a decrease in their chain size, likely due to decreasing electrostatic repulsions with decreasing polarity. However, the comparison of the specific viscosity scaling with PAA concentration show a similar polyelectrolyte-like scaling $\eta_{sp} \sim c^{0.5}$ at low concentrations (semi-dilute unentangled regime) for all IPA% suggesting electrostatic interactions are predominantly controlling their properties at dilute concentrations despite a reduction in the solvent polarity by IPA.

Whereas at higher concentrations, in both the semi-dilute entangled and concentrated regimes, increasing IPA % increases their scaling, and reduces the entanglement concentration. Their scaling exponent increases from $n \sim 1.68$ to 2 in the entangled regime and from 4.14 to 5.6 in the concentration regime with increasing IPA from 25% to 75%. The scaling exponents increasingly deviate from salt-free polyelectrolytes solutions, which are predicted to be $n \sim 1.5$ and $n \sim 3.75$ in the entangled and concentrated regime. Such trends suggest an increasing trend in the degree of PAA aggregation with increasing IPA. The specific viscosities and moduli at intermediate IPA% however display a maximum, qualitatively similar to previous findings on PAA and NaCMC solutions in water-alcohol mixtures. Such non-monotonic trend indicates a maximum PAA aggregation at intermediate alcohol fractions.

The scaling of the extensional relaxation time with concentration, $\lambda_E \sim c^n$, in the unentangled and entangled regime for the PAA solutions at intermediate alcohol fraction (50% IPA) was examined. In both regimes, their scaling was found to be stronger compared to previous reports on PAA solutions in water, where $n \sim 0.76$ in the unentangled and $n \sim 3.42$ in the entangled regime. And the comparison of their relaxation times as a function of IPA% in the semi-dilute entangled regime at fixed PAA concentrations showed a monotonic increase in the extensional relaxation time with increasing IPA%, indicating that IPA enhances the stability of the filaments in extensional flows. Such trend however deviates from shear rheology, which in contrast showed a maximum in their shear viscosities and moduli, suggesting that a complex interplay of multiple interactions controls their structure, affecting their shear and extensional flow response differently.

Electrospinning experiments showed both the onset of the beaded fiber and uniform fiber morphologies reduces with increasing IPA%, consistent with previous findings. Such trends are in a better agreement, qualitatively, with increasing trend of the dimensionless Deborah number than Ohnesorge number, which instead varies non-monotonically with increasing IPA%. Such agreement suggests that enhancement of the elasticity of PAA solutions by IPA and resulting stabilizing effect on their filaments/jets in electrospinning, is playing a role in the improvement of their fiber formation.

Further comparison of the onset of both beaded fibers and uniform fibers relative to the entanglement concentration of the PAA solutions showed $C_{fb} \sim 0.5 \times C_e$ and $C_f \sim 2 \times C_e$, respectively, which are much lower compared to the previous findings on salt-free polyelectrolyte solutions. Additional analysis using global dimensionless number, the elasto-capillary number where $Ec > Ec_c \sim 4.7$ for all the solutions, suggested that this discrepancy is due to the predominantly elastic nature of the PAA solutions. This is likely due to the relatively higher molecular weight of the PAA used in this study compared to the previous studies on polyelectrolytes solutions. The intrinsic Deborah numbers corresponding to the onset of beaded fibers and uniform fibers, $De_{0,fb} > 5$ for and $De_{0,f} > 22$, respectively, are also found to larger compared to previous reports on neutral polymers, due to the reduced extensional viscosities of polyelectrolytes solutions compared to neutral polymers likely arising from electrostatic interactions which reduce the flexibility of polyelectrolyte structure. Nevertheless, the comparisons suggest the onset for fiber formation relative to the entanglement concentration of polyelectrolyte solutions, which are often larger compared to neutral polymers, could be significantly reduced by increasing the molecular weights, because of an enhancement of their elasticity.

Our findings show that the addition alcohol-cosolvent fraction enhances the elasticity of aqueous PAA solutions, and the resulting stabilizing effect on the jets/filaments during the electrospinning process improves the fiber formation. These findings provide guidance for optimizing broad polyelectrolyte formulations, enabling the fabrication of electrospun nanofibers for a range of applications.

26424169, 2023, 14, Downloaded from https://onlinelibrary.wiley.com/doi/10.1002/pol.20220719 by National Renewable Energy Lab, Wiley Online Library on [27/07/2023]. See the Terms and Conditions (https://onlinelibrary.wiley.com/terms-and-conditions) on Wiley Online Library for rules of use; OA articles are governed by the applicable Creative Commons License

ACKNOWLEDGMENTS

The authors thank the reviewers for critical comments and suggestions toward improving the manuscript quality, and Paul Meyer and Carlos Baez-Cotto for discussions and assistance with polymer characterization. This work was authored by Alliance for Sustainable Energy, LLC, the manager and operator of the National Renewable Energy Laboratory for the U.S. Department of Energy (DOE) under Contract No. DE-AC36-08GO28308. Funding provided by U.S. Department of Energy, Office of Energy Efficiency and Renewable Energy, Advanced Manufacturing Office. The views expressed in the article do not necessarily represent the views of the DOE or the U.S. Government. The U.S. Government retains and the publisher, by accepting the article for publication, acknowledges that the U.S. Government retains a nonexclusive, paid-up, irrevocable, worldwide license to publish or reproduce the published form of this work, or allow others to do so, for U.S. Government purposes.

DATA AVAILABILITY STATEMENT

Data available on request from the authors.

ORCID

Sunilkumar Khandavalli https://orcid.org/0000-0003-3179-5718

REFERENCES

[1] R. Faturechi, A. Karimi, A. Hashemi, H. Yousefi, M. Navidbakhsh, *Adv. Polym. Technol.* **2015**, 34.
[2] L. Meng, W. Klinkajon, P. K-hasuwan, S. Harkin, P. Supaphol, G. E. Wnek, *Polym. Int.* **2015**, *64*, 42.
[3] B. Ding, M. Yamazaki, S. Shiratori, *Sens Actuat B: Chem* **2005**, *106*, 477.
[4] Y. Liu, M. Park, B. Ding, J. Kim, M. El-Newehy, S. S. Al-Deyab, H. Y. Kim, *Fibers Polym.* **2015**, *16*, 629.
[5] K. A. Hays, R. E. Ruther, A. J. Kukay, P. Cao, T. Saito, D. L. Wood, J. Li, *J. Power Sources* **2018**, *384*, 136.
[6] H. Chen, Y. L. Hsieh, *Biotechnol. Bioeng.* **2005**, *90*, 405.
[7] I. Ismail, N. F. A. Bakar, T. H. Ling, N. Ideris, Z. H. M. Zain, N. Radacsi, *Mater. Today: Proc.* **2019**, *17*, 574.
[8] D. H. Reneker, A. L. Yarin, *Polymer* **2008**, *49*, 2387.
[9] W. E. Teo, S. Ramakrishna, *Nanotechnology* **2006**, *17*, R89.
[10] S. Cavaliere, S. Subianto, I. Savych, D. J. Jones, J. Rozière, *Energy Environ. Sci.* **2011**, *4*, 4761.
[11] P. Gupta, G. L. Wilkes, *Polymer* **2003**, *44*, 6353.
[12] S. L. Shenoy, W. D. Bates, H. L. Frisch, G. E. Wnek, *Polymer* **2005**, *46*, 3372.
[13] S. A. Theron, E. Zussman, A. L. Yarin, *Polymer* **2004**, *45*, 2017.
[14] J. H. Yu, S. V. Fridrikh, G. C. Rutledge, *Polymer* **2006**, *47*, 4789.
[15] M. G. McKee, G. L. Wilkes, R. H. Colby, T. E. Long, *Macromolecules* **2004**, *37*, 1760.
[16] L. Palangetic, N. K. Reddy, S. Srinivasan, R. E. Cohen, G. H. McKinley, C. Clasen, *Polymer* **2014**, *55*, 4920.
[17] C. D. Saquing, C. Tang, B. Monian, C. A. Bonino, J. L. Manasco, E. Alsberg, S. A. Khan, *Ind. Eng. Chem. Res.* **2013**, *52*, 8692.
[18] M. G. McKee, M. T. Hunley, J. M. Layman, T. E. Long, *Macromolecules* **2006**, *39*, 575.
[19] S. Y. Tsou, H. S. Lin, C. Wang, *Polymer* **2011**, *52*, 3127.
[20] S.-Y. Tsou, H.-S. Lin, P.-J. Cheng, C.-L. Huang, J.-Y. Wu, C. Wang, *Eur. Polym. J.* **2013**, *49*, 3619.
[21] C. Subramanian, R. A. Weiss, M. T. Shaw, *Polymer* **2010**, *51*, 1983.
[22] M. E. Helgeson, K. N. Grammatikos, J. M. Deitzel, N. J. Wagner, *Polymer* **2008**, *49*, 2924.
[23] C. Clasen, J. P. Plog, W.-M. Kulicke, M. Owens, C. Macosko, L. E. Scriven, M. Verani, G. H. McKinley, *J. Rheol.* **2006**, *50*, 849.
[24] S. L. Shenoy, W. D. Bates, G. Wnek, *Polymer* **2005**, *46*, 8990.
[25] M. G. McKee, C. L. Elkins, T. E. Long, *Polymer* **2004**, *45*, 8705.
[26] H. Chen, J. D. Snyder, Y. A. Elabd, *Macromolecules* **2008**, *41*, 128.
[27] A. V. Dobrynin, R. H. Colby, M. Rubinstein, *Macromolecules* **1996**, *28*, 1859.
[28] R. H. Colby, *Rheol. Acta* **2010**, *49*, 425.
[29] H. Nie, A. He, J. Zheng, S. Xu, J. Li, C. C. Han, *Biomacromolecules* **2008**, *9*, 1362.
[30] S. P. Pandey, T. Shukla, V. K. Dhote, D. K. Mishra, R. Maheshwari, R. K. Tekade, *Basic Fundamentals of Drug Delivery.* Elsevier Inc, Academic Press **2019**, pp. 113, Ch. 4.
[31] Y. Park, S. Lee, S. S. Ha, B. Alunda, D. Y. Noh, Y. J. Lee, S. Kim, J. H. Seol, *Polymer* **2019**, *11*, 858.
[32] L. Li, Y. L. Hsieh, *Nanotechnology* **2005**, *16*, 2852.
[33] B. Kim, H. Park, S.-H. Lee, W. M. Sigmund, *Mater. Lett.* **2005**, *59*, 829.
[34] S. Vats, L. W. Honaker, M. W. Frey, F. Basoli, J. P. F. Lagerwall, *Macromol. Mater. Eng.* **2022**, *307*, 2100640.
[35] S. V. Ebadi, A. Fakhrali, D. Semnani, *Bull. Mater. Sci.* **2019**, *42*, 115.
[36] S. Khandavalli, N. Sharma-Nene, S. Kabir, S. Sur, J. P. Rothstein, K. C. Neyerlin, S. A. Mauger, M. Ulsh, *ACS Appl. Polym. Mater.* **2021**, *3*, 2374.
[37] J. Chong, S. Xun, H. Zheng, X. Song, G. Liu, P. Ridgway, J. Q. Wang, V. S. Battaglia, *J. Power Sources* **2011**, *196*, 7707.
[38] L. Li, Y.-L. Hsieh, *Polymer* **2005**, *46*, 5133.
[39] S. Kabir, T. V. Cleve, S. Khandavalli, S. Medina, S. Pylypenko, S. Mauger, M. Ulsh, K. C. Neyerlin, *ACS Appl. Energy Mater.* **2021**, *4*, 3341.
[40] H. Fong, I. Chun, D. H. Reneker, *Polymer* **1999**, *40*, 4585.
[41] B. Veleirinho, M. F. Rei, J. A. Lopes-DA-Silva, *J. Polym. Sci. Part B: Polym. Phys.* **2008**, *46*, 460.
[42] W. K. Son, J. H. Youk, T. S. Lee, W. H. Park, *Polymer* **2004**, *45*, 2959.
[43] J. Merchiers, C. D. V. Martínez Narváez, C. Slykas, N. K. Reddy, V. Sharma, *Macromolecules* **2021**, *54*, 11061.
[44] S. Kheirandish, I. Gubaydullin, N. Willenbacher, *Rheol. Acta* **2009**, *48*, 397.
[45] L. N. Jimenez, J. Dinic, N. Parsi, V. Sharma, *Macromolecules* **2018**, *51*, 5191.
[46] L. N. Jimenez, C. D. V. Martínez Narváez, V. Sharma, *Macromolecules* **2022**, *55*, 8117.
[47] L. N. Jimenez, C. D. V. Martínez Narváez, V. Sharma, *Phys. Fluids* **2020**, *32*, 012113.
[48] H. Choi, J. R. Mitchell, S. R. Gaddipati, S. E. Hill, B. Wolf, *Food Hydrocolloids* **2014**, *40*, 71.
[49] S. Różańska, J. Różański, *Soft Mater.* **2017**, *15*, 302.

26424169, 2023, 14, Downloaded from https://onlinelibrary.wiley.com/doi/10.1002/pol.20220719 by National Renewable Energy Lab, Wiley Online Library on [27/07/2023]. See the Terms and Conditions (https://onlinelibrary.wiley.com/terms-and-conditions) on Wiley Online Library for rules of use; OA articles are governed by the applicable Creative Commons License

[50] S. Różańska, K. Verbeke, J. Różański, C. Clasen, P. Wagner, *J. Polym. Sci. Part B: Polym. Phys.* **2019**, *57*, 1537.
[51] A. V. Walter, L. N. Jimenez, J. Dinic, V. Sharma, K. A. Erk, *Rheol. Acta* **2019**, *58*, 145.
[52] J. Slack, B. Halevi, G. McCool, J. Li, R. Pavlicek, R. Wycisk, S. Mukerjee, P. Pintauro, *ChemElectroChem* **2018**, *5*, 1537.
[53] G. H. Chen, D. Kelly, A. Shine, Z. Liu, L. Wang, S. Bliznakov, M. Rafailovich, *MRS Commun.* **2019**, *9*, 1343.
[54] S. Khandavalli, J. P. Rothstein, *J. Rheol.* **2014**, *58*, 411.
[55] S. Sur, J. Rothstein, *J. Rheol.* **2018**, *62*, 1245.
[56] G. Vazquez, E. Alvarez, J. M. Navaza, *J. Chem. Eng. Data* **1995**, *40*, 611.
[57] D. T. Papageorgiou, *Phys. Fluids* **1995**, *7*, 1529.
[58] V. M. Entov, E. J. Hinch, *J. Non-Newton. Fluid Mech.* **1997**, *72*, 31.
[59] T. T. Ngo, T. L. Yu, H. L. Lin, *J. Power Sources* **2013**, *225*, 293.
[60] S. Khandavalli, R. Iyer, J. H. Park, D. J. Myers, K. C. Neyerlin, M. Ulsh, S. A. Mauger, *Langmuir* **2020**, *36*, 12247.
[61] C. Wandrey, *Langmuir* **1999**, *15*, 4069.
[62] D. Truzzolillo, F. Bordi, C. Cametti, S. Sennato, *Phys. Rev. E* **2009**, *79*, 011804.
[63] C. G. Lopez, R. H. Colby, P. Graham, J. T. Cabral, *Macromolecules* **2017**, *50*, 332.
[64] N. B. Wyatt, M. W. Liberatore, *J. Appl. Polym. Sci.* **2009**, *114*, 4076.
[65] G. S. Manning, *Q. Rev. Biophys.* **1978**, *11*, 179.
[66] M. G. Mckee, M. T. Hunley, J. M. Layman, T. E. Long, *Macromolecules* **2006**, *39*, 575.
[67] U. Kästner, H. Hoffmann, R. Dönges, J. Hilbig, *Colloids Surf. Physicochem. Eng. Asp.* **1997**, *123–124*, 307.
[68] A. Dodero, S. Vicini, M. Alloisio, M. Castellano, *Rheol. Acta* **2020**, *59*, 365.
[69] M. Muthukumar, *Macromolecules* **2017**, *50*, 9528.
[70] G. S. Manning, *Eur. Phys. J. E: Soft Matter Biol. Phys.* **2011**, *34*, 132.
[71] M. Muthukumar, *J. Chem. Phys.* **1996**, *105*, 5183.
[72] J. Ray, G. S. Manning, *Macromolecules* **2000**, *33*, 2901.
[73] H. Schiessel, P. Pincus, *Macromolecules* **1998**, *31*, 7953.
[74] J. J. Tanahatoe, M. E. Kuil, *J. Phys. Chem. B* **1997**, *101*, 5905.
[75] B. D. Ermi, E. J. Amis, *Macromolecules* **1998**, *31*, 7378.
[76] J. J. Tanahatoe, M. E. Kuil, *J. Phys. Chem. B* **1997**, *101*, 10839.
[77] Y. Zhang, J. F. Douglas, B. D. Ermi, E. J. Amis, *J. Chem. Phys.* **2001**, *114*, 3299.
[78] R. Borsali, H. Nguyen, R. Pecora, *Macromolecules* **1998**, *31*, 1548.
[79] B. V. R. Tata, N. Ise, *Phys. Rev. E* **1998**, *58*, 2237.
[80] N. Grønbech-Jensen, R. J. Mashl, R. F. Bruinsma, W. M. Gelbart, *Phys. Rev. Lett.* **1997**, *78*, 2477.
[81] A. Varghese, R. Rajesh, S. Vemparala, *J. Chem. Phys.* **2012**, *137*, 234901.
[82] A. M. Tom, R. Rajesh, S. Vemparala, *J. Chem. Phys.* **2017**, *147*, 144903.
[83] B. Hammouda, F. Horkay, M. L. Becker, *Macromolecules* **2005**, *38*, 2019.
[84] M. Guettari, A. Belaidi, S. Abel, T. Tajouri, *J. Solution Chem.* **2017**, *46*, 1404.
[85] R. Shankar, R. R. Klossner, J. T. Weaver, T. Koga, J. H. van Zanten, W. E. Krause, C. M. Colina, F. Tanaka, R. J. Spontak, *Soft Matter* **2009**, *5*, 304.
[86] J. Merchiers, C. D. V. Martínez Narváez, C. Slykas, M. Buntinx, W. Deferme, J. D'Haen, R. Peeters, V. Sharma, N. K. Reddy, *J. Polym. Sci.* **2021**, *59*, 2754.
[87] J. W. Bye, C. L. Freeman, J. D. Howard, G. Herz, J. McGregor, R. J. Falconer, *J. Solution Chem.* **2017**, *46*, 175.
[88] J. McGregor, R. Li, J. A. Zeitler, C. D'Agostino, J. H. P. Collins, M. D. Mantle, H. Manyar, J. D. Holbrey, M. Falkowska, T. G. A. Youngs, C. Hardacre, E. H. Stitt, L. F. Gladden, *Phys. Chem. Chem. Phys.* **2015**, *17*, 30481.
[89] R. Li, C. D'Agostino, J. McGregor, M. D. Mantle, J. A. Zeitler, L. F. Gladden, *J. Phys. Chem. B* **2014**, *118*, 10156.
[90] S. L. Anna, G. H. McKinley, *J. Rheol.* **2001**, *45*, 115.
[91] G. H. Mckinley, *Soc. Rheol. Bull* **2005**, *2005*, 6.
[92] J. Dinic, V. Sharma, *Macromolecules* **2020**, *53*, 3424.
[93] R. F. Fedors, *Polymer* **1979**, *20*, 225.
[94] L. Ghimici, F. Popescu, *Eur. Polym. J.* **1998**, *34*, 13.
[95] O. Arnolds, H. Buggisch, D. Sachsenheimer, N. Willenbacher, *Rheol. Acta* **2010**, *49*, 1207.
[96] J. Dinic, M. Biagioli, V. Sharma, *J. Polym. Sci. Part B: Polym. Phys.* **2017**, *55*, 1692.
[97] J. Dinic, V. Sharma, *Macromolecules* **2020**, *53*, 4821.
[98] S. J. Haward, V. Sharma, C. P. Butts, G. H. McKinley, S. S. Rahatekar, *Biomacromolecules* **2012**, *13*, 1688.
[99] S. H. Spiegelberg, G. H. McKinley, *J. Non-Newton. Fluid Mech.* **1996**, *67*, 49.
[100] C. Clasen, P. M. Phillips, L. Palangetic, J. Vermant, *AIChE J.* **2012**, *58*, 3242.
[101] Y. Wang, T. Hashimoto, C. C. Li, Y. C. Li, C. Wang, *J. Polym. Sci. Part B: Polym. Phys.* **2018**, *56*, 319.
[102] E. Ewaldz, J. Randrup, B. Brettmann, *ACS Polym.* **2022**, *2*, 108.
[103] A. Y. Malkin, A. V. Semakov, I. Y. Skvortsov, P. Zatonskikh, V. G. Kulichikhin, A. V. Subbotin, A. N. Semenov, *Macromolecules* **2017**, *50*, 8231.
[104] J. Merchiers, N. K. Reddy, V. Sharma, *Macromolecules* **2022**, *55*, 942.
[105] S. Tripatanasuwan, Z. Zhong, D. H. Reneker, *Polymer* **2007**, *48*, 5742.

SUPPORTING INFORMATION

Additional supporting information can be found online in the Supporting Information section at the end of this article.

How to cite this article: S. Khandavalli, Y. Chen, N. Sharma-Nene, K. S. Rajan, S. Sur, J. P. Rothstein, K. S. Reeves, D. A. Cullen, K. C. Neyerlin, S. A. Mauger, M. Ulsh, *J. Polym. Sci.* **2023**, *61*(14), 1495. https://doi.org/10.1002/pol.20220719

26424169, 2023, 14, Downloaded from https://onlinelibrary.wiley.com/doi/10.1002/pol.20220719 by National Renewable Energy Lab, Wiley Online Library on [27/07/2023]. See the Terms and Conditions (https://onlinelibrary.wiley.com/terms-and-conditions) on Wiley Online Library for rules of use; OA articles are governed by the applicable Creative Commons License